


## Spin diffusion and spin conductivity in the two-dimensional Hubbard model

Martin Ulaga<sup>1</sup>,<sup>✉</sup> Jernej Mravlje,<sup>1</sup> and Jure Kokalj<sup>2,1</sup>

<sup>1</sup>*Jozef Stefan Institute, Jamova 39, SI-1000 Ljubljana, Slovenia*

<sup>2</sup>*Faculty of Civil and Geodetic Engineering, University of Ljubljana, Jamova 2, Ljubljana, Slovenia*

 (Received 11 November 2020; revised 22 February 2021; accepted 6 April 2021; published 14 April 2021)

We study the spin diffusion and spin conductivity in the square lattice Hubbard model by using the finite-temperature Lanczos method. We show that the spin diffusion behaves differently from the charge diffusion and has a nonmonotonic  $T$  dependence. This is due to a progressive liberation of charges that contribute to spin transport and enhance it beyond that active at low temperature due to the Heisenberg exchange. We further show that going away from half filling and zero magnetization increases the spin diffusion, but that the increase is insufficient to reconcile the difference between the model calculations and the recent measurements on cold atoms.

DOI: [10.1103/PhysRevB.103.155123](https://doi.org/10.1103/PhysRevB.103.155123)

### I. INTRODUCTION

Nonsaturating metallic resistivity  $\rho$  that exceeds the Mott-Ioffe-Regel (MIR) value (estimated with the scattering length  $l$  equal to the lattice spacing,  $l \sim a$ ) is a characteristic property of strongly correlated metals. Recent theoretical work [1,2] found that within the Hubbard model, such behavior of conductivity  $\sigma_c = 1/\rho$  can be understood via the Nernst-Einstein relation  $\sigma_c = D_c \chi_c$ , with a saturating diffusion constant  $D_c$  and strongly suppressed charge susceptibility at elevated temperatures. Cold-atom experiments [3] have verified this behavior, which established that at least the high-temperature regime of the charge transport is fully understood.

Simultaneously, cold atoms were also used to probe much less explored quantities: The spin conductivity  $\sigma_s$  and spin diffusion constant  $D_s$  [4] (the spin current that flows as a response to the magnetic field or magnetization gradient). These quantities are not only important from a theoretical point of view (as the interplay between spins and charges lies at the heart of the strong-correlation problem [5,6]) but are important also, e.g., for the applications in spintronics [7–9], for heat transfer [10–12], and further to understand the behavior of the NMR relaxation rate [13–15].  $\sigma_s$  or  $D_s$  can be indirectly estimated via heat conductivity or the NMR relaxation rate, but also more directly through the spin injection technique [16–18] and magnetization current measurements [19,20].

Importantly, in correlated materials, the spins and charges do not behave alike and they exhibit a so-called spin-charge separation [5,6], which means one cannot infer the behavior of spin degrees of freedom (e.g.,  $\sigma_s$ ,  $D_s$ , and  $\chi_s$ ), based on the measurements of charge properties (e.g.,  $\sigma_c$ ,  $D_c$ , and  $\chi_c$ ), and vice versa. The question that arises is, how strong is the spin-charge separation in different temperature ( $T$ ) regimes? Can one understand also the spin transport more simply in terms of the Nernst-Einstein relation? Does  $D_s$  saturate and to what value? The cold-atom experiment [4] has not analyzed this behavior in detail, and, intriguingly, reported an inconsistency with the numerical linked-cluster expansion (NLCE) method.

In this paper we consider these questions by solving the Hubbard model with the finite-temperature Lanczos method (FTLM). We find that spin transport at high  $T$  can be understood in terms of the Nernst-Einstein relation, but the behavior is richer than the one for the charge transport.  $D_s$  has a nonmonotonic  $T$  dependence and experiences an increase at high  $T$  on the crossover between two saturated regimes: The lower- $T$  one at  $T$  of the order of Heisenberg exchange  $J$  with strong spin-charge separation and the asymptotic high- $T$  one, where the spins and charges behave alike. The scattering length remains of the order of lattice spacing throughout this crossover and the behavior is explained in terms of the evolution of effective velocity, instead.

Previously, the spin diffusion in two-dimensional (2D) lattices was considered for the Heisenberg model, namely with high- $T$  frequency moments [13,21], with the theory of Blume and Hubbard [22], with the interacting spin-wave theory [23,24], and with the numerical [25] and Mori-Zwanzig [14] approach to the  $t$ - $J$  model. The spin diffusion in the Hubbard model was considered with a Gaussian extrapolation of short-time dynamics in the weak-coupling limit [26], and with NLCE [4]. To our knowledge, the  $T$  dependence of  $D_s$  in the Hubbard model has yet to be numerically calculated.

This paper is structured as follows: We briefly present the method in Sec. II and then present the results for dynamical conductivity in Sec. III and for spin diffusion in Sec. IV. We comment on a phenomenological explanation for these results in Sec. V and comment on the effect of doping and magnetization in Sec. VI. Appendix A contains a derivation of the sum rule for dynamical spin conductivity while Appendixes B, C, and E contain further details on the calculated quantities.

### II. MODEL AND METHOD

We consider the Hubbard model on the square lattice,

$$H = -t \sum_{\langle i,j \rangle, s} c_{i,s}^\dagger c_{j,s} + U \sum_i n_{i,\uparrow} n_{i,\downarrow}, \quad (1)$$

where  $c_{i,s}^\dagger/c_{i,s}$  create/annihilate an electron of spin  $s$  (either  $\uparrow$  or  $\downarrow$ ) at the lattice site  $i$ .  $t$  is the hopping amplitude between the nearest neighbors and we use it as the energy units. We further set  $\hbar = k_B = e = g\mu_B = 1$ . We denote the lattice constant with  $a$ .

We solve the model with FTLM [27–29], which uses the Lanczos algorithm to obtain the approximate eigenstates of the Hamiltonian and additional sampling over the initial random vectors to treat finite- $T$  properties on small clusters. We use an  $N = 4 \times 4$  cluster. To reduce the finite-size effects that appear at  $T < t$  we further employ averaging over twisted boundary conditions and use the grand canonical ensemble. This allows us to reach reliable results, e.g., for  $U = 10t$ , at  $T \gtrsim 0.2t$  for the thermodynamic quantities (e.g., spin susceptibility  $\chi_s$ ), and at  $T \gtrsim 0.8t$  for dynamical quantities (e.g., dc spin conductivity  $\sigma_s$ ). We omit low- $T$  results for which, due to finite size, dynamical spin stiffness exceeds 1% of the total spectral weight.

To calculate  $D_s$  (and analogously the charge diffusion constant  $D_c$ ) we use the Nernst-Einstein relation (see, e.g., Refs. [26,30] for a derivation)

$$\sigma_s = D_s \chi_s. \quad (2)$$

The dc spin conductivity  $\sigma_s$  is calculated as the  $\omega = 0$  value of the dynamical spin conductivity  $\sigma_s(\omega)$ , which is directly evaluated as the current-current correlation function [1,27].  $\sigma_s(\omega)$  for a finite cluster consists of delta functions which need to be broadened. This introduces some uncertainty in dynamical results and we estimate the uncertainty due to finite-size effects and broadening to be  $\lesssim 10\%$ .

### III. DYNAMICAL CONDUCTIVITY

In Figs. 1(a)–1(c) we show the dynamical spin  $\sigma_s(\omega)$  and charge  $\sigma_c(\omega)$  conductivities for the half-filled Hubbard model

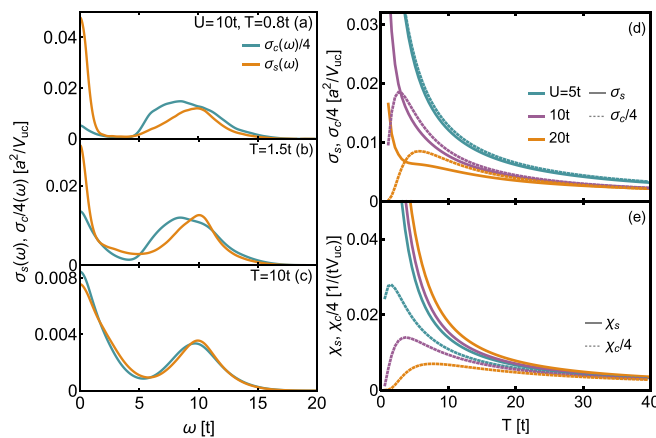


FIG. 1. Dynamical spin conductivity  $\sigma_s(\omega)$  and charge conductivity  $\sigma_c(\omega)$ . (a) At low  $T$ ,  $\sigma_s(\omega)$  shows a large Drude-like peak and the conducting character, while  $\sigma_c(\omega)$  shows an insulating behavior with only a small value at  $\omega \sim 0$ . (b) At an intermediate temperature  $J < T < U$ , a low- $\omega$  peak in  $\sigma_s(\omega)$  develops a shoulderlike structure. (c) At high  $T$ ,  $\sigma_s(\omega)$  and  $\sigma_c(\omega)$  become similar. (d) Comparison of  $\sigma_s$  and  $\sigma_c$ , which are similar for  $T \gtrsim U/2$ , and (e) comparison of  $\chi_s$  and  $\chi_c$ . Results are for half filling ( $p = 1 - n = 0$ ).

at half filling for  $U = 10t$ . The two quantities behave very similarly at high  $T$ , and both display a low- $\omega$  “Drude” peak, and a high- $\omega$  peak at  $\omega \sim U$  due to transitions to Hubbard bands.

On cooling down, there is a growing degree of the spin-charge separation. The charge transport is depleted and the low- $\omega$  peak in  $\sigma_c(\omega)$  is suppressed, corresponding to the Mott-insulating regime. Conversely, in the spin conductivity, a peak develops at  $\omega \sim 0$ , corresponding to a spin-metallic regime in the spin sector [see also Fig. 1(d) for the  $T$  dependence of the dc transport]. The two quantities  $\sigma_s(\omega)$  and  $\sigma_c(\omega)$  are actually never fully independent as they are related by the  $f$ -sum rule. Namely, their integrals over frequency are equal up to a factor of 4 [31] as we show in Appendix A. This also means that at low  $T$ , parts of the spectral weight in  $\sigma_s(\omega)$  are in comparison to  $\sigma_c(\omega)$  removed from the Hubbard band to accommodate the increase at low  $\omega$ . One can relate the behavior of  $\sigma_{c,s}(\omega)$  to charge and spin fluctuations, e.g.,  $\sigma_{c,s}(\omega) = \lim_{q \rightarrow 0} \frac{\omega}{q^2} \text{Im}[\chi_{c,s}(q, \omega)]$ . Here,  $\chi_{c,s}(q, \omega)$  are the dynamical susceptibilities. Relative to the charge sector, on lowering  $\omega$ , the spin fluctuations are first suppressed and then increased. One can also notice that  $\sigma_s(\omega)$  at intermediate  $T$  develops an interesting two-peak-like structure at  $\omega \sim 0$  [see Fig. 1(b)], i.e., a sharper peak on top of the broader peak both centered at  $\omega = 0$ . Notice also that whereas the key distinction between the behavior of spins and charges could be expected at the energy scales of the order of the Heisenberg exchange  $J = 4t^2/U$ , the two conductivities differ also at larger energy scales.

It is worth mentioning that the difference between  $\sigma_s(\omega)$  and  $\sigma_c(\omega)$  vanishes at the bubble level and appears due to the vertex correction (see, e.g., Refs. [31–33]). Their difference is therefore a direct indication of the importance of vertex corrections.

In Fig. 1(e) we show also the  $T$  dependence of spin and charge susceptibilities  $\chi_{s,c}$ . One sees a clear distinction between  $\chi_c$  that decreases at low  $T$ , indicating a charge gap, and large values of  $\chi_s$ , indicating a large local moment and a Curie-Weiss-like behavior. See Appendix C for more details.

### IV. SPIN DIFFUSION

We now turn to the  $T$  dependence of the diffusion constant. Figure 2(a) shows  $D_s$  vs  $T$  for several  $U$ . Even though the spin conductivities are all metallic,  $D_s$  shows an unusual nonmonotonic  $T$  dependence. Unlike in the case of charge transport in metals (where  $D_c$  monotonously increases with lowering  $T$ ),  $D_s$  initially drops, reaches a minimum, and only at the lowest available  $T$  starts to grow. The growth of  $D_s$  in this low- $T$  regime can be discussed in terms of a growing correlation length and associated coherence of spin waves in the Heisenberg model [22,34] and associated longer mean free path  $l_s$  (as  $D_s \sim v_s l_s/2$  with  $v_s$  a characteristic spin velocity). To indicate the expected behavior, we supplement our results in Fig. 2(a) with a result of Nagao *et al.* [22] for the Heisenberg model.

At intermediate  $T$  ( $\sim 2t$ ),  $D_s$  reaches a minimum with indications for intermediate saturating behavior seen for larger  $U$ . In the regime of  $T \ll U$  for large  $U$ , the behavior becomes that of the Heisenberg model and is therefore entirely controlled by  $J$ . The calculated  $D_s$  hence agrees with the results

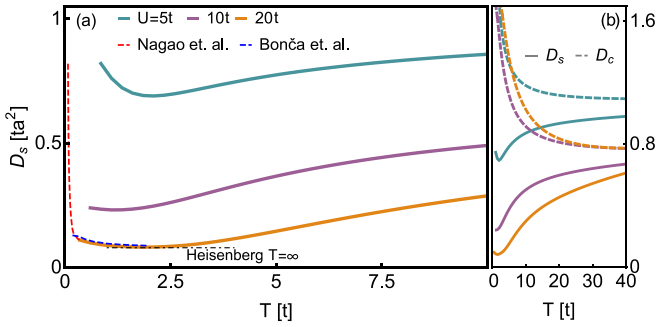


FIG. 2. (a) Spin diffusion constant  $D_s$  for a half-filled Hubbard model for  $U/t = 5, 10, 20$ .  $D_s$  decreases with increasing  $U$  and shows a nonmonotonic  $T$  dependence. As  $T \rightarrow 0$ , one expects a diverging  $D_s$  due to the increased spin coherence [22,25,26], which shows up as a small upturn in our results. The divergence is indicated by showing the result of a Blume and Hubbard theory for the Heisenberg model for Nagao *et al.* [22] for  $U = 20t$ . In the intermediate regime  $J \ll T \ll U$ ,  $D_s$  is minimal and for large  $U$  shows a saturating behavior corresponding to the high- $T$  Heisenberg result [13] and agrees with the FTLM result for the Heisenberg model [25]. (b) As  $T$  increases further,  $D_s$  shows an increase and saturates for  $T \rightarrow \infty$  at the same value as the charge diffusion  $D_c$  and in accordance with the standard Mott-Ioffe-Regel limit.

from the Heisenberg model, including high- $T$  moment expansion [13], numerical FTLM [25], and with the self-consistent Blume and Hubbard theory [22].  $D_s$  further shows in a regime  $J \ll T \ll U$  a saturation towards the high- $T$  limit of the Heisenberg model [13,25] with  $D_s \sim 0.40Ja^2$  [see results for  $U = 20t$  in Fig. 2(a)]. Such a high- $T$  value can be understood in terms of a “spin Mott-Ioffe-Regel” value by approximating the spin-wave velocity to  $v_s \sim \frac{4Ja}{\sqrt{2\pi}}$  and  $l_s$  to a minimal or MIR limiting value  $l_s \sim a$ . This leads to  $D_s \sim v_s l_s / 2 \sim 0.45Ja^2$ .

With a further increase of  $T$  towards  $U$ ,  $D_s$  remarkably increases. This is in contradiction with a naive expectation of a decreasing mean free path (increasing scattering rate) and therefore decreasing  $D_s$  with increasing  $T$ . The reason for this can be found in the increase of empty and doubly occupied sites allowing for a new conducting and diffusive mechanism of spin in terms of electron hopping, in addition to the exchange mechanism dominating at low  $T$ .

Figure 2(b) additionally shows the charge diffusion constants compared to  $D_s$  in a broader  $T$  range. One notices that  $D_c$  decreases on heating up (which is the standard behavior) and that  $D_c$  and  $D_s$  approach each other at very high  $T$ . There, both  $D_s$  and  $D_c$  saturate at the usual MIR limit  $D \sim at^2$ .

It is interesting to observe that in a broad temperature regime  $T \gtrsim U/2$  the conductivities  $\sigma_s$  and  $\sigma_c$  differ little (<20%) [Fig. 1(d)], while the corresponding diffusion constants differ by a factor of almost 2 [Fig. 2(b)]. The difference between  $D_s$  and  $D_c$  is compensated by the inverse difference between susceptibilities  $\chi_s$  and  $\chi_c$  [Fig. 1(e)] to give similar conductivities in the whole  $T \gtrsim U/2$  regime. This suggests an intriguing relationship between the diffusion (dynamic) and susceptibility (static property).

In passing we mention also that in the high- $T$  limit ( $T \gg U$ ),  $D_s$  does not show the  $t^2/U$  scaling, as suggested from the moment expansion analysis [26]. This can be traced

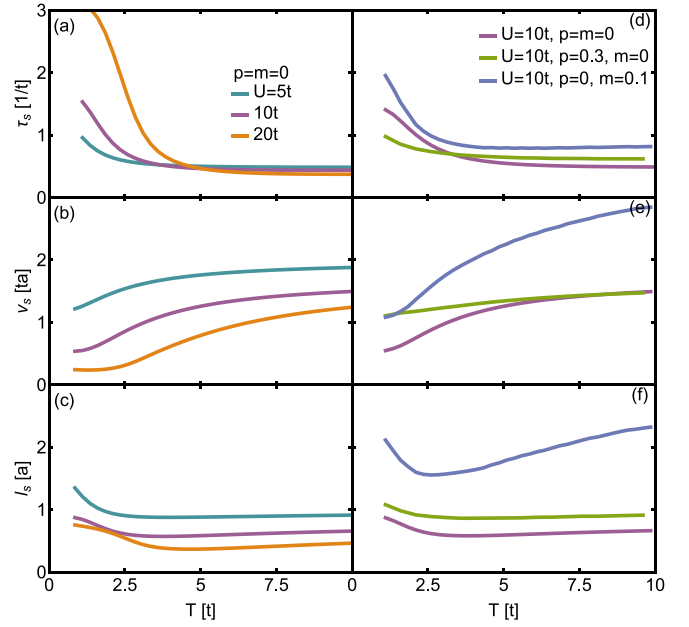


FIG. 3.  $T$  dependence of spin scattering time  $\tau_s$ , spin velocity  $v_s$ , and spin mean free path  $l_s$  for several choices of interaction strength  $U$ , hole doping  $p$ , and magnetization  $m$ .

back to the two-peak structure in the dynamical spin conductivity (Fig. 1) with the upper Hubbard peak positioned at  $\omega \sim U$ , which is quite challenging to correctly reproduce from the frequency moments.

## V. MEAN FREE PATH

It is instructive to investigate the phenomenology of our results in more detail. From the width of the low-frequency peak in  $\sigma_s(\omega \sim 0)$  [e.g., Figs. 1(a)–1(c)] we estimate a spin scattering time  $\tau_s$  (see also Appendix E). Then we use a simple relation  $D_s \sim \frac{v_s^2 \tau_s}{2}$  and the values of  $D_s$  to estimate the spin velocity  $v_s$  and further the spin mean free path  $l_s \sim v_s \tau_s$ . The results are plotted in Fig. 3, and reveal the evolution between two regimes, a lower- $T$  one governed by the scale  $J$  and a higher- $T$  one governed by  $t$ .  $\tau_s$  is seen to exhibit a pronounced increase below  $T \sim U/2$ , which coincides with a sharp structure of width  $1/\tau_s \sim J$  emerging in the dynamical spectra. At  $T \gtrsim U/2$  it saturates at a value of order  $1/\tau_s \sim t$ . The extracted characteristic velocity starts at values  $v_s \sim Ja$  at low  $T$  and increases monotonically to the value of  $v_s \sim ta$ . The low- $T$  estimate of  $v_s \sim 0.6ta$  for  $U = 10t$  [Fig. 3(b)] is remarkably close to the estimate of  $v_s \sim 1.6Ja \sim 0.64ta$  within the Heisenberg model [35], in particular, since we used a rough approximation  $D_s \sim v_s^2 \tau_s / 2$ .

Conversely,  $l_s$  is to a good approximation  $T$  independent and close to the lattice spacing. It shows only a moderate increase at lowest  $T$ . The spin transport is thus characterized by a saturated scattering length throughout the considered  $T$  regime (except at lowest  $T$ ) and the effects seen in the diffusion constant are explained in terms of a progressive unbinding of the charge degrees of freedom that progressively increase the corresponding velocity to a value given by  $t$  instead of  $J$ . In the half-filled case, this increase of  $v_s$  is the

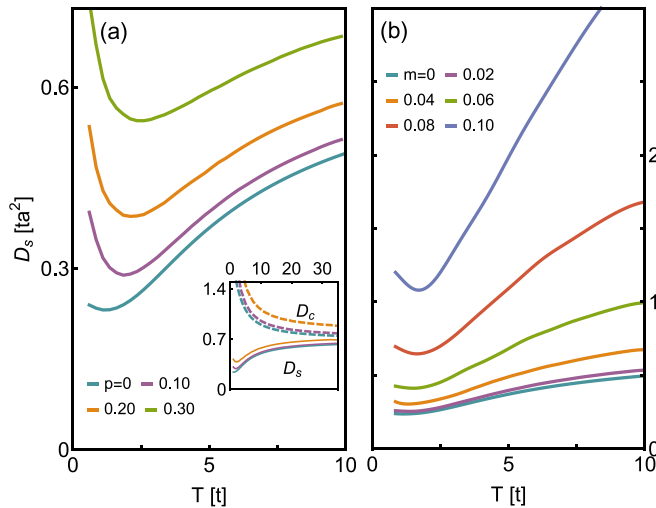


FIG. 4. (a) Increase of spin diffusion  $D_s$  with doping  $p$ . Inset: In the whole shown  $T$  and  $p$  regime  $D_s$  is smaller and behaves qualitatively differently than  $D_c$ , even at largest  $p = 0.3$ . They become similar only in the very high  $T$  limit.  $U = 10t$ . (b)  $D_s$  vs  $T$  for several values of magnetizations  $m$ . With increasing  $m$ ,  $D_s$  increases in the whole  $T$  range.  $U = 10t$ ,  $p = 0$ .

main reason for the increase of  $D_s \sim v_s l_s / 2$  with increasing  $T$  (see Fig. 2). We note that the dependence of  $l_s$  on  $U$  in Fig. 2(c) is smaller at higher  $T (> U)$  and  $l_s$  is closer to  $a$  for all  $U$ .

## VI. DOPING AND MAGNETIZATION EFFECT

How is this picture modified at finite dopings and magnetizations? Because moving electrons carry both spin and charge, one could expect that away from half filling, when the system is metallic,  $D_s$  and  $D_c$  behave more similarly. In Fig. 4(a) we show the behavior of  $D_s$  for several dopings  $p = 1 - n$ .  $n$  is the electron density. One clearly observes the increase of  $D_s$  with increasing  $p$ , which is understood as the opening of a new conducting channel via the hopping of itinerant electrons or holes. The increase is particularly strong at the lowest calculated  $T$  and the indication of diverging  $D_s(T \rightarrow 0)$  becomes more apparent. In the doped case,  $D_s$  approaches  $D_c$ , but  $D_s$  and  $D_c$  still behave distinctly [Fig. 4 (inset)], with  $D_s$  having much smaller values and a pronounced minimum at intermediate  $T$ . Thus, doping diminishes the degree of spin-charge separation, but does not wash it out completely. At low  $T$ ,  $D_s$  is much smaller than  $D_c$  and the spin transport is less coherent than the charge transport, possibly due to a stronger coupling to low-lying spin excitations. The extracted  $l_s$  remains roughly  $T$  independent [Fig. 3(f)] and is somewhat larger, but still  $l_s \sim a$ . The extracted  $v_s$  and  $\tau_s$  show less  $T$  dependence than in the undoped case [Figs. 3(d) and 3(e)].

The dependence on magnetization  $m = \langle S_{z,\text{tot}} \rangle / N$  is shown in Fig. 4(b). It is found to be initially weak but becomes strong with increasing  $m$ . The results for  $m = 0.1$  deviate significantly from the nonmagnetized ones, e.g.,  $D_s$  is increased by more than a factor of 4. The underlying physics differs from the case of charge doping: With increasing  $m$  one stays in, or even goes deeper into, the Mott-insulating phase (see Figs. 1

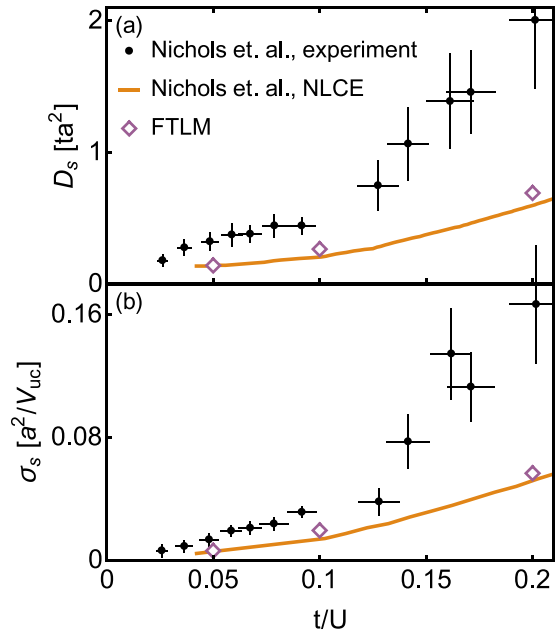


FIG. 5. Comparison of our FTLM results with experimental data [4] and numerical NLCE results [4]. FTLM results are for a fixed entropy density of  $1.1k_B$ , which was estimated for the experiment and taken also in the NLCE calculations.

and 2 in Ref. [36]). The increase of  $D_s$  is therefore not due to mobile electronlike particles, but rather due to a weaker scattering of spin waves and their longer  $l_s$ . This is indeed revealed in Fig. 3(f), where  $l_s$  is increased due to an increase of both  $v_s$  and  $\tau_s$ . With increasing  $m$  the Hubbard interaction becomes less effective and one approaches the limit of noninteracting spins or a single noninteracting holon-doublon pair [36] (the limit of only one  $\downarrow$  spin in the background of  $\uparrow$  spins). The strong increase of  $D_s$  with increasing  $T$  at  $T \gtrsim 2t$  is mainly due to increasing  $v_s$ , but surprisingly, also  $l_s$  moderately increases with increasing  $T$  as well.

## VII. DISCUSSION

We compared our results to the  $D_s$  and  $\sigma_s$  measured in the cold-atom experiment [4] (see Fig. 5), where the measured  $D_s$  and  $\sigma_s$  are found to be by about a factor of 2 higher than the NLCE results for the Hubbard model. Our results agree well with the NLCE results. As discussed in Sec. VI,  $D_s$  and  $\sigma_s$  are increased by magnetization. We estimate that the experimental deviation from half filling and zero magnetization are too small to understand the discrepancy between the numerics and experiment in those terms.

We also compare (see Appendix D) our results with the diffusion bound  $D_s > v_s^2 / T$  suggested from holographic duality [37]. Using our rough estimate for  $v_s$  extracted from  $D_s$  and  $\tau_s$ , we observe that the bound is obeyed in most of the explored parameter regime except at small  $U$ , where it is mildly violated. See also Ref. [30].



### VIII. CONCLUSIONS

We have shown that  $D_s$  has a striking nonmonotonic  $T$  dependence, which can be understood in terms of a crossover from a low- $T$  spin-wave dominated regime to a high- $T$  asymptotic regime via an intermediate strong spin-charge separation regime, where it nearly saturates according to the high- $T$  Heisenberg model result at  $D_s \sim Ja^2$ . In both of these high- $T$  regimes, the scattering length is of the order of the lattice spacing and the conductivity is strongly reduced due to decreased  $\chi_s$ . In analogy to the case of charge transport, these regimes can be referred to as a *spin bad metal*. The action in  $D_s$  is governed by the spin velocity that evolves from  $J$  to  $t$  up to the asymptotic high- $T$  regime, where spins and charges behave alike and  $D_s \sim D_c \sim ta^2$ .

In the whole regime of  $T \lesssim U/2$  (with or without doping or magnetization) the spins and charges behave differently. An interesting open question is a better characterization of the behavior at lower  $T$ . Away from half filling in the well-defined quasiparticle regime one expects similar behavior of the spin and charge transport. Further studies in real materials, e.g., with techniques such as spin injection [16–18] or magnetization current measurements [19,20], would be highly valuable. A better understanding of the spin transport would also shed light on the thermal conductivity and NMR relaxation rate [38], for which our results suggest a nonmonotonic-in- $T$  diffusive contribution.

### ACKNOWLEDGMENTS

We acknowledge helpful discussions with Peter Prelovšek, Friedrich Krien, Matthew A. Nichols, and Martin W. Zwierlien. This work was supported by the Slovenian Research Agency (ARRS) under Program No. P1-0044.

### APPENDIX A: SUM RULE

To derive the spectral sum rule for the dynamical spin conductivity we employ the approach by Shastry [39]. The sum rule is given by the expectation value of the stress tensor  $\mathcal{T}$ ,

$$\int_{-\infty}^{\infty} \sigma_{c,s}(\omega) d\omega = \frac{\pi \langle \mathcal{T}_{c,s} \rangle}{N}. \quad (\text{A1})$$

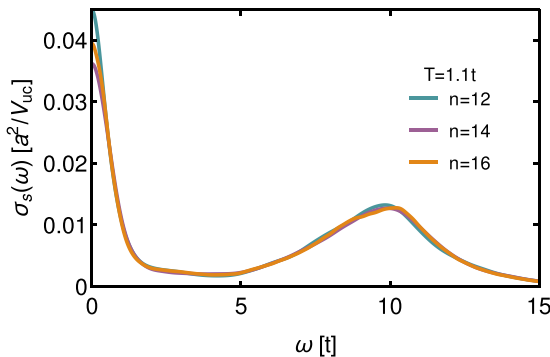


FIG. 6. Comparison of the optical spectrum of spin conductivity obtained on different size clusters. We use 16 different periodic boundary conditions for  $N = 12$  and  $N = 14$  and 8 for  $N = 16$ .

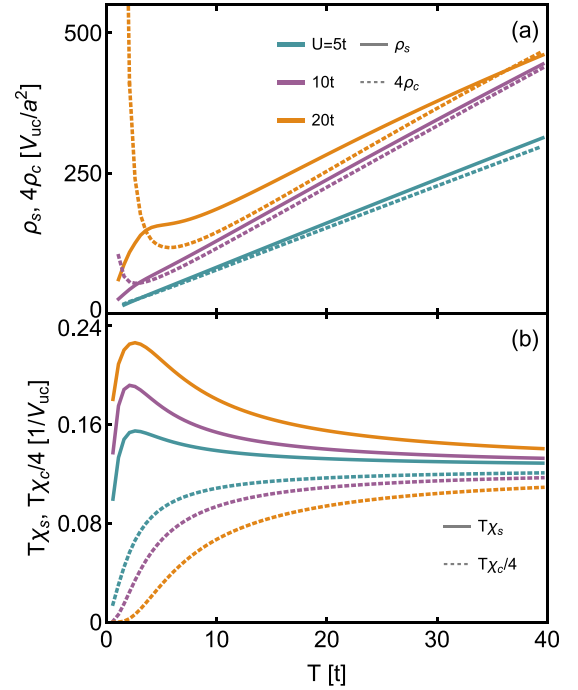


FIG. 7. (a) Spin and charge resistivities. The latter is multiplied by 4 to aid the comparison. (b) Spin and charge susceptibilities multiplied by temperature.

Subscripts  $c$  and  $s$  stand for charge and spin quantities, respectively. The charge stress tensor is given by [39]

$$\mathcal{T}_c = - \lim_{q \rightarrow 0} \frac{d}{dq} [j_c(q), n(-q)], \quad (\text{A2})$$

where the charge current and charge density operators are

$$j_c(q) = it \sum_{i,\delta,s} \delta_x c_{i+\delta,s}^\dagger c_{i,s} e^{iq(R_{i,x} + \delta_x/2)}, \quad (\text{A3})$$

$$n(q) = \sum_{i,s} n_{i,s} e^{iqR_{i,x}}. \quad (\text{A4})$$

Here, the  $x$  direction of current and of the wave vector  $q$  is explicitly used.  $\delta$  goes over all nearest neighbors and  $\delta_x$  denotes the spatial distance to the neighboring site in the  $x$  direction.  $R_{i,x}$  is the  $x$  coordinate of site  $i$ . Similarly, one can write the spin stress tensor,

$$\mathcal{T}_s = - \lim_{q \rightarrow 0} \frac{d}{dq} [j_s(q), m(-q)], \quad (\text{A5})$$

and the spin current and magnetization density operators,

$$j_s(q) = it \sum_{i,\delta,s} s \delta_x c_{i+\delta,s}^\dagger c_{i,s} e^{iq(R_{i,x} + \delta_x/2)}, \quad (\text{A6})$$

$$m(q) = \sum_{i,s} s n_{i,s} e^{iqR_{i,x}}. \quad (\text{A7})$$

Here, the factor  $s$  in the sums for  $j_s(q)$  and  $m(q)$  is taken to be  $1/2$  for  $\uparrow$  spins and  $-1/2$  for  $\downarrow$  spins. Evaluating the commutation in expressions for  $\mathcal{T}_c$  in Eq. (A2) and for  $\mathcal{T}_s$  in

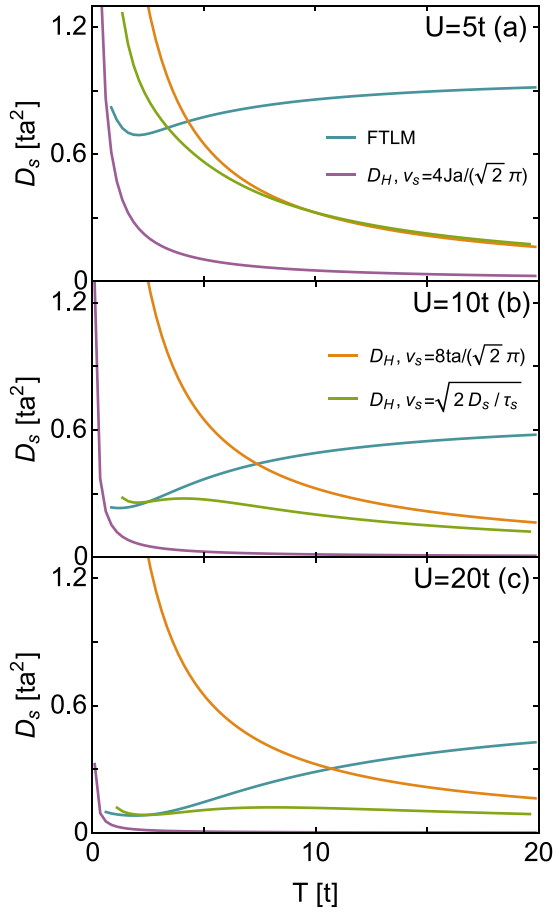


FIG. 8. Comparison of  $D_s$  calculated with FTLM results for various  $U$  to the conjectured diffusion bound [37]  $D_H = v_s^2/T$ . If the bound is valid, the calculated  $D_s$  (denoted with FTLM) would be larger than  $D_H$ . Due to uncertainty of  $v_s$ , which is needed to evaluate  $D_H$ , we compare to three values of  $D_H$  obtained with three estimates for  $v_s$ . Our best estimate of  $v_s$  is obtained via  $\tau_s$  and the corresponding  $D_H$  is shown with a green line. At lowest  $T$ , our results indicate possible violation of the proposed bound.

Eq. (A5) together with the  $q$  derivative and limit, one obtains similar expressions for  $\mathcal{T}_c$  and  $\mathcal{T}_s$ ,

$$\mathcal{T}_c = t \sum_{i,\delta,s} \delta_x^2 c_{i+\delta,s}^\dagger c_{i,s}, \quad (\text{A8})$$

$$\mathcal{T}_s = t \sum_{i,\delta,s} s^2 \delta_x^2 c_{i+\delta,s}^\dagger c_{i,s}. \quad (\text{A9})$$

The reason for the only difference of factor  $s^2 = 1/4$  in the expression for  $\mathcal{T}_s$  (A9), in comparison with  $\mathcal{T}_c$  (A8), is the commutation of spin  $\uparrow$  and  $\downarrow$  operators and no spin mixed terms in the sums for currents and density operators [Eqs. (A3), (A4), (A6), and (A7)]. The expectation values of  $\mathcal{T}_c$  and  $\mathcal{T}_s$  correspond to the expectation values of the kinetic energy for our nearest-neighbor Hubbard model [27]

$$\langle \mathcal{T}_c \rangle = \frac{a^2}{2} \langle H_{\text{kin}} \rangle, \quad (\text{A10})$$

$$\langle \mathcal{T}_s \rangle = \frac{a^2}{8} \langle H_{\text{kin}} \rangle. \quad (\text{A11})$$

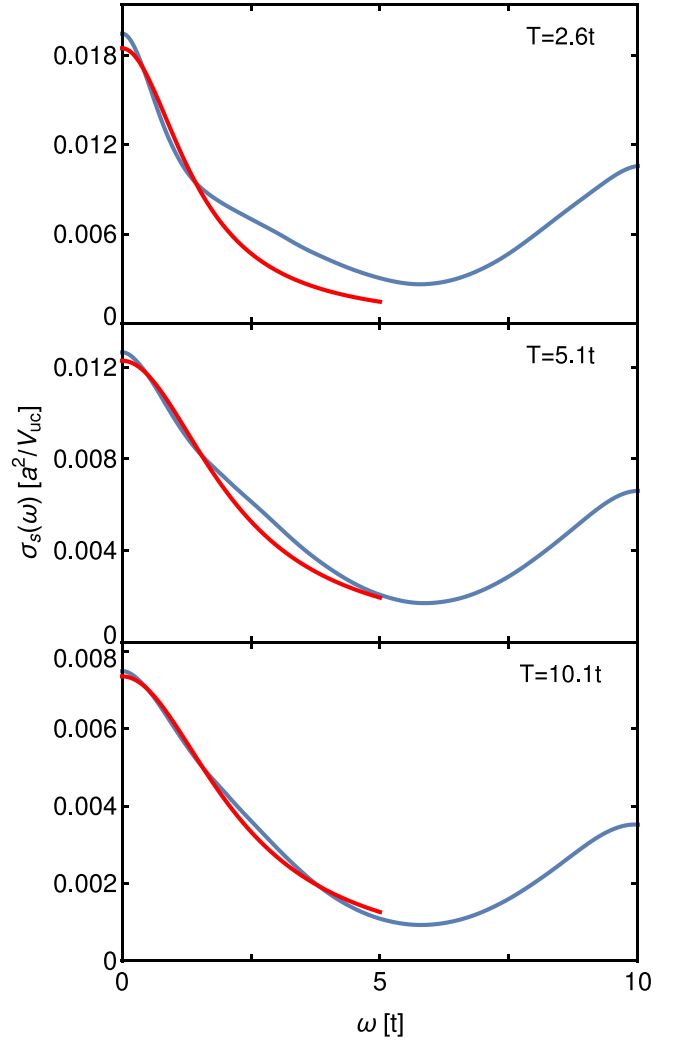


FIG. 9. Lorentz curve fitted to the low- $\omega$  structure in  $\sigma_s(\omega)$  for  $U = 10$  and several  $T$ . For fitting we consider only  $\omega \leq 2t$ . We estimate the uncertainty of the extracted scattering time to be  $\sim 30\%$  at low  $T$  and  $\sim 5\%$  at  $T \gtrsim U/2$ .

This leads to the (optical) sum rule given in the main text,

$$\int_{-\infty}^{\infty} \sigma_c(\omega) d\omega = \frac{\pi a^2}{2N} \langle H_{\text{kin}} \rangle, \quad (\text{A12})$$

$$\int_{-\infty}^{\infty} \sigma_s(\omega) d\omega = \frac{\pi a^2}{8N} \langle H_{\text{kin}} \rangle, \quad (\text{A13})$$

with the difference only of a factor of  $1/4$ .

## APPENDIX B: FINITE-SIZE EFFECTS

To estimate the error due to finite-size effects, we plot the optical spin conductivity for different system sizes in Fig. 6. We find that they differ substantially only around  $\omega = 0$ . This is the basis for the error estimate given in the main text.

## APPENDIX C: RESISTIVITY

It is instructive to inspect also the inverse conductivity, namely the resistivity  $\rho = 1/\sigma$ . See Fig. 7(a). Linear-in- $T$

resistivity is easily recognized for both  $\rho_c$  and  $\rho_s$  at high  $T$  and  $\rho_c$  shows a pronounced crossover into the insulating regime at low  $T$ , while  $\rho_s$  remains metallic. Spin susceptibility  $\chi_s$  shows [Fig. 7(b)] an increase below  $T \sim U$  and approaches the value of the high- $T$  Heisenberg limit with  $T\chi_s = 1/4$ , which is expected for large  $U$  and  $J \ll T \ll U$ . In the ultrahigh  $T$  limit,  $T \gg U$ , both  $T\chi_s$  and  $T\chi_c/4$  approach the atomic limit of  $1/8$ .

#### APPENDIX D: DIFFUSION BOUND

We compare FTLM results to the conjectured lower bound on diffusion [37], given by

$$D_s \gtrsim D_H = \frac{v_s^2}{T}, \quad (\text{D1})$$

for some characteristic velocity  $v_s$ . While we cannot directly evaluate the velocity, we can estimate it using the noninteractinglike models. We take  $v_s = \frac{4Ja}{\sqrt{2\pi}}$  as a typical velocity of spins deep in the Mott-insulating phase and  $v_s = \frac{8ta}{\sqrt{2\pi}}$  as a typical speed of electrons. The real velocity is expected to be close to and interpolate between these two values. Our best estimate of velocity  $v_s$  is obtained via calculation of  $D_s$  and  $\tau_s$  (see Fig. 9) and using the approximate relation  $D_s = v_s^2\tau_s/2$  as discussed in the main text. We use these three velocities to estimate the various diffusion bounds and compare them with our FTLM results in Fig. 8.

We observe no apparent violation of the bound for  $v_s = \frac{4Ja}{\sqrt{2\pi}}$ , a strong violation of the bound for  $v_s = \frac{8ta}{\sqrt{2\pi}}$ , while for our best estimate of  $v_s = \sqrt{2D_s/\tau_s}$  there is an indication of a diffusion bound violation at lowest  $T$ . It is most apparent for  $U = 5t$ , as shown in Fig. 8(a). However, due to a rough estimate of  $v_s$ , we do not consider this as a clearcut violation. We do, however, remark that the proposed bound does not manifest in any clear way in our results (in distinction with the Mott-Ioffe-Regel value).

#### APPENDIX E: SCATTERING TIME

To estimate the spin scattering time, we fit the Lorentz curve to the low- $\omega$  part of  $\sigma_s(\omega)$ . For illustration, see Fig. 9. We choose to fit in the frequency range from  $\omega = 0$  to  $\omega = 2t$ . Due to the dependence of the extracted width ( $1/\tau_s$ ) on the frequency range and other possible prescriptions, e.g., taking the half width at half maximum, our value of  $\tau_s$  should be taken as a rough estimate. We estimate its uncertainty to about 30%, and to be largest at lowest  $T$ . This uncertainty is then translated also to the uncertainty in the spin velocity  $v_s$  and mean free path  $l_s$ . We note that the spectra at low  $\omega$  are a bit sharper and more linear than the Lorentz curve. Quite linear-in- $\omega$  behavior was, e.g., observed in the optical conductivity for the  $t$ - $J$  model [27], where a comparable  $\omega$  resolution can be reached with a smaller number of Lanczos steps. For a recent discussion, see Ref. [40].

- 
- [1] J. Kokalj, *Phys. Rev. B* **95**, 041110(R) (2017).
- [2] E. Perepelitsky, A. Galatas, J. Mravlje, R. Žitko, E. Khatami, B. S. Shastry, and A. Georges, *Phys. Rev. B* **94**, 235115 (2016).
- [3] P. T. Brown, D. Mitra, E. Guardado-Sanchez, R. Nourafkan, A. Reymbaut, C.-D. Hébert, S. Bergeron, A.-M. S. Tremblay, J. Kokalj, D. A. Huse, P. Schauß, and W. S. Bakr, *Science* **363**, 379 (2019).
- [4] M. A. Nichols, L. W. Cheuk, M. Okan, T. R. Hartke, E. Mendez, T. Senthil, E. Khatami, H. Zhang, and M. W. Zwierlein, *Science* **363**, 383 (2019).
- [5] P. W. Anderson, *Phys. Today* **50**(10), 42 (1997).
- [6] P. A. Lee, N. Nagaosa, and X.-G. Wen, *Rev. Mod. Phys.* **78**, 17 (2006).
- [7] I. Žutić, J. Fabian, and S. Das Sarma, *Rev. Mod. Phys.* **76**, 323 (2004).
- [8] A. V. Chumak, V. I. Vasyuchka, A. A. Serga, and B. Hillebrands, *Nat. Phys.* **11**, 453 (2015).
- [9] A. Hirohata, K. Yamada, Y. Nakatani, I.-L. Prejbeanu, B. Diény, P. Pirro, and B. Hillebrands, *J. Magn. Magn. Mater.* **509**, 166711 (2020).
- [10] X. Zotos, F. Naef, and P. Prelovšek, *Phys. Rev. B* **55**, 11029 (1997).
- [11] A. V. Sologubenko, K. Giannò, H. R. Ott, A. Vietkine, and A. Revcolevschi, *Phys. Rev. B* **64**, 054412 (2001).
- [12] C. Hess, C. Baumann, U. Ammerahl, B. Büchner, F. Heidrich-Meisner, W. Brenig, and A. Revcolevschi, *Phys. Rev. B* **64**, 184305 (2001).
- [13] A. Sokol, E. Gagliano, and S. Bacci, *Phys. Rev. B* **47**, 14646 (1993).
- [14] I. A. Larionov, *Phys. Rev. B* **69**, 214525 (2004).
- [15] E. Yusuf, B. J. Powell, and R. H. McKenzie, *Phys. Rev. B* **75**, 214515 (2007).
- [16] M. Johnson, *Phys. Rev. Lett.* **70**, 2142 (1993).
- [17] Q. Si, *Phys. Rev. Lett.* **78**, 1767 (1997).
- [18] Y. Ji, A. Hoffmann, J. S. Jiang, and S. D. Bader, *App. Phys. Lett.* **85**, 6218 (2004).
- [19] F. Meier and D. Loss, *Phys. Rev. Lett.* **90**, 167204 (2003).
- [20] L. J. Cornelissen, J. Liu, R. A. Duine, J. B. Youssef, and B. J. van Wees, *Nat. Phys.* **11**, 1022 (2015).
- [21] H. S. Bennett and P. C. Martin, *Phys. Rev.* **138**, A608 (1965).
- [22] T. Nagao and J.-i. Igarashi, *J. Phys. Soc. Jpn.* **67**, 1029 (1998).
- [23] M. Sentef, M. Kollar, and A. P. Kampf, *Phys. Rev. B* **75**, 214403 (2007).
- [24] A. S. T. Pires and L. S. Lima, *Phys. Rev. B* **79**, 064401 (2009).
- [25] J. Bonča and J. Jaklič, *Phys. Rev. B* **51**, 16083 (1995).
- [26] P. Kopietz, *Phys. Rev. B* **57**, 7829 (1998).
- [27] J. Jaklič and P. Prelovšek, *Adv. Phys.* **49**, 1 (2000).
- [28] P. Prelovšek and J. Bonča, *Strongly Correlated Systems: Numerical Methods*, edited by A. Avella and F. Mancini, Springer Series in Solid-State Sciences (Springer, Berlin, 2013).
- [29] J. Kokalj and R. H. McKenzie, *Phys. Rev. Lett.* **110**, 206402 (2013).
- [30] N. Pakhira and R. H. McKenzie, *Phys. Rev. B* **91**, 075124 (2015).

- [31] R. S. Fishman and M. Jarrell, *J. Appl. Phys.* **91**, 8120 (2002).
- [32] J. Vučićević, J. Kokalj, R. Žitko, N. Wentzell, D. Tanasković, and J. Mravlje, *Phys. Rev. Lett.* **123**, 036601 (2019).
- [33] A. Vranić, J. Vučićević, J. Kokalj, J. Skolimowski, R. Žitko, J. Mravlje, and D. Tanasković, *Phys. Rev. B* **102**, 115142 (2020).
- [34] S. Chakravarty, B. I. Halperin, and D. R. Nelson, *Phys. Rev. B* **39**, 2344 (1989).
- [35] J.-K. Kim and M. Troyer, *Phys. Rev. Lett.* **80**, 2705 (1998).
- [36] P. Prelovšek, J. Kokalj, Z. Lenarčič, and R. H. McKenzie, *Phys. Rev. B* **92**, 235155 (2015).
- [37] S. A. Hartnoll, *Nat. Phys.* **11**, 54 (2015).
- [38] M. Takigawa, T. Asano, Y. Ajiro, M. Mekata, and Y. J. Uemura, *Phys. Rev. Lett.* **76**, 2173 (1996).
- [39] B. S. Shastry, *Rep. Prog. Phys.* **72**, 016501 (2008).
- [40] C. Schönle, D. Jansen, F. Heidrich-Meisner, and L. Vidmar, [arXiv:2011.13958](https://arxiv.org/abs/2011.13958).